BBA - General Subjects 1864 (2020) 129506

Contents lists available at ScienceDirect

BBA - General Subjects

journal homepage: www.elsevier.com/locate/bbagen

Dehydrin ERD14 activates glutathione transferase Phi9 in *Arabidopsis thaliana* under osmotic stress

Phuong N. Nguyen[a,b,c,j,1], Maria-Armineh Tossounian[a,b,k,1], Denes S. Kovacs[a,b], Tran T. Thu[a,b], Benoit Stijlemans[e,f], Didier Vertommen[g], Jarne Pauwels[h,i], Kris Gevaert[h,i], Geert Angenon[j], Joris Messens[a,b,k,*], Peter Tompa[a,b,d,*]

[a] VIB-VUB Center for Structural Biology (CSB), Vlaams Instituut voor Biotechnologie (VIB), Brussels, Belgium
[b] Structural Biology Brussels (SBB), Vrije Universiteit Brussel (VUB), 1050 Brussels, Belgium
[c] Department of Biology, College of Natural Sciences, Cantho University, Viet Nam
[d] Institute of Enzymology, Research Centre for Natural Sciences of the Hungarian Academy of Sciences, Budapest, Hungary
[e] Lab of Cellular and Molecular Immunology, Vrije Universiteit Brussel (VUB), 1050 Brussels, Belgium
[f] Myeloid Cell Immunology Lab, VIB Center for Inflammation Research, Brussels, Belgium
[g] de Duve Institute, Université Catholique de Louvain, 1200 Brussels, Belgium
[h] VIB-UGent Center for Medical Biotechnology, University of Ghent, B9000 Ghent, Belgium
[i] Department of Biomolecular Medicine, University of Ghent, B9000 Ghent, Belgium
[j] Laboratory of Plant Genetics (PLAN), Vrije Universiteit Brussel (VUB), Brussels, Belgium
[k] Brussels Center for Redox Biology, 1050 Brussels, Belgium

ARTICLE INFO

Keywords:
Oxidative stress
Chaperone
Hydrogen peroxide
Enzyme activation
Intrinsically disordered protein
Active site titration

ABSTRACT

Background: Fully intrinsically disordered plant dehydrin ERD14 can protect enzymes via its chaperone-like activity, but it was not formally linked with enzymes of the plant redox system yet. This is of particular interest, as the level of H_2O_2 in *Arabidopsis* plants increases during osmotic stress, which can be counteracted by over-expression of ERD14.

Methods: The proteomic mass-spectrometry analysis of stressed plants was performed to find the candidates affected by ERD14. With cross-linking, microscale thermophoresis, and active-site titration kinetics, the interaction and influence of ERD14 on the function of two target proteins: glutathione transferase Phi9 and catalase was examined.

Results: Under osmotic stress, redox enzymes, specifically the glutathione transferase Phi enzymes, are upregulated. Using microscale thermophoresis, we showed that ERD14 directly interacts with GSTF9 with a K_D of ~25 μM. ERD14 activates the inactive GSTF9 molecules, protects GSTF9 from oxidation, and can also increases the activity of the enzyme. Aside from GSTF9, we found that ERD14 can also interact with catalase, an important cellular H_2O_2 scavenging enzyme, with a K_D of ~0.13 μM, and protects it from dehydration-induced loss of activity.

Conclusions: We propose that fully intrinsically disordered dehydrin ERD14 might protect and even activate redox enzymes, helping plants to survive oxidative stress under dehydration conditions.

General significance: ERD14 has a direct effect on the activity of redox enzymes.

1. Introduction

In plants under osmotic stress, the hydrogen peroxide (H_2O_2) level increases, which could lead to protein, lipid, and DNA damage [1–3]. H_2O_2 can inactivate some enzymes, like for example, dehydratases [4] and peroxidases [5]. Hence, plant cells have developed multiple lines of defense mechanisms [6,7] to control and maintain cellular redox homeostasis. In particular, plants accumulate stress metabolites and

Abbreviations: FMS, full-strength Murashige & Skoog; PBS_T, PBS buffer with 0,1% Tween 20; ERD14 OE, ERD14 overexpressing; ERD14 KO, ERD14 knockout; MS, mass spectrometry; GST, glutathione transferase; CAT, catalase

* Corresponding authors at: VIB-VUB Center for Structural Biology, Vlaams Instituut voor Biotechnologie (VIB), Vrije Universiteit Brussel (VUB), Pleinlaan 2, 1050 Brussels, Belgium.
E-mail addresses: joris.messens@vub.be (J. Messens), peter.tompa@vub.be (P. Tompa).
[1] These authors have contributed equally to this work

https://doi.org/10.1016/j.bbagen.2019.129506
Received 18 August 2019; Received in revised form 12 December 2019; Accepted 18 December 2019
Available online 20 December 2019

anti-oxidant enzymes, such as catalase, superoxide dismutase, and ascorbate peroxidase [7]. Another important line of defense under osmotic stress is the upregulation of specific proteins such as late embryogenesis abundant (LEA) proteins, desiccation stress proteins (DSP), and dehydrins [8].

Although not yet directly linked to oxidative damage response, LEA proteins have been suggested to improve plant survival under osmotic and oxidative stress conditions [9,10] through several mechanisms, such as membrane stabilization [11,12], free-radical scavenging [13], and direct chaperone action [14]. Dehydrins represent one of the major groups of LEA proteins, which accumulate during seed desiccation and also in response to water deficit induced by drought or salt stress [15,16]. A high content of polar residues makes that most of the dehydrins are intrinsically disordered proteins (IDPs) [17]. Dehydrins in different plant species are defined and classified by the presence and architecture of conserved sequence motifs, termed lysine-rich (K-), and serine-rich [18] segments [19]. Conserved K-segments (consensus sequence EKKGIMDKIKEKLPG [11]) give these dehydrins a high potential to protect proteins under oxidative stress [20]. For example, K-segments were shown to be indispensable for dehydrins for their protective function to prevent enzyme denaturation [17,21]. K-segments also have been shown to form amphipathic helical structures [19], which might be essential in protecting cellular macromolecules and lipid membranes [22,23].

Due to their highly hydrophilic amino acid composition, most dehydrins are IDPs [9] that can protect their clients by various chaperone-like mechanisms, such as space filling/molecular shield or entropy transfer [24]. The Early Response to Dehydration 14 (ERD14) of *A. thaliana* belongs to the class 2 LEA proteins (dehydrins) that have a K_2S domain architecture [23]. ERD14 and it paralogue, ERD10, with which it shares about 70% sequence identity, are potent chaperones, protecting enzymes, such as alcohol dehydrogenase, citrate synthase, lysozyme, and firefly luciferase, against the loss of activity and aggregation [14,25,26], and they can play a role in protecting plants exposed to cold and drought stress [27]. Whereas ERD14 was shown to have chaperone activity, it has not yet been linked to oxidative damage response through either activating or protecting redox enzymes.

Here, we show that ERD14 has a protective role against oxidative stress elicited by dehydration. We show the activation of glutathione transferase Phi9 (GSTF9) catalysis by ERD14, which could mitigate oxidative damage caused by H_2O_2 during dehydration stress. The action of ERD14 on GSTF9 might even be a more general mechanism for redox enzymes, as we found that ERD14 also protects catalase under dehydration conditions.

2. Experimental procedures

2.1. Generation of ERD14 overexpressing and knockout plants

ERD14 OE and KO lines were generated from *Arabidopsis* Col-0 ecotype. For ERD14 overexpression, a fragment containing the coding region, which was amplified by genomic PCR with primers ERD14-attB1 and ERD14-attB2 (Supplementary Table 1), was cloned into pDON^{R}221 donor vector. Then, it was cloned into the destination vector pk7CWG2.0 to fuse with CFP under the control of the 35S promoter. The ERD14 OE transgenic *Arabidopsis* line was obtained by *Agrobacterium*-mediated floral-dip method [28], and verified by PCR with specific primers. The primer sequences can be found in Supplementary Table 1. The ERD14 KO line seeds with NASC code N857331 were ordered from Nottingham Arabidopsis Stock Centre (NASC).

2.2. Plant material

Arabidopsis seeds were surface sterilized and placed on full-strength Murashige & Skoog (FMS) medium [29] supplemented with the appropriate antibiotics (50 mg/L kanamycin for ERD14 OE plants, and 15 mg/L phosphinothricin for ERD14 KO plants). Seeds were stratified at 4 °C for two days before transferring them to the culture room (23 ± 2 °C; 16 h/8 h light/dark). OE and KO seeds were screened for two generations to get the homozygous seeds. One-week old seedlings germinating on FMS agar were transferred to conditions appropriate for the actual experimental design.

2.3. ERD14 expression and purification

ERD14 was purified as described by Kovacs et al. [14] with minor modifications. Briefly, ERD14 expressing BL21(DE3) cells were induced by 0.7 mM IPTG. Cells were collected, lysed in lysis buffer (50 mM Tris pH 8.0, 150 mM NaCl, 1 mM benzamidine (BA), 0.5 mM phenylmethylsulfonyl fluoride (PMSF), 5 mg DNase I, 20 mM $MgCl_2$ and protease inhibitor cocktail (Roche)), and then sonicated for 3 min (10 s pulse on, 10 s pulse off, 60% amplitude) using Sonics Vibra Cell. After centrifuging (20 min, 20,000 xg and 4 °C), the supernatant was boiled for 20 min to remove globular proteins. The lysate was then desalted using HiPrep™ 26/10 desalting column equilibrated with buffer A (50 mM Tris pH 8.0, 0.05 mM BA, 0.05 mM PMSF). The collected fractions were pooled and loaded onto a HiTrap DEAE Sepharose FF column (GE Healthcare Life Sciences). Following washing with buffer A, ERD14 was eluted with a gradient of 10 to 500 mM NaCl in buffer A. The purification was repeated one more time on a MonoQ (4.6–100) column to remove all contaminants. The samples were analyzed on SDS-PAGE gel and stored at −20 °C.

2.4. Isolation of anti-ERD14 specific antibodies

Serum from recombinant-ERD14 immunized mice was passed over a protein G column (GE Healthcare Life Sciences) and polyclonal IgG was eluted using 0.1 M glycine-HCl, pH 2.7. Following overnight dialysis against PBS the concentration of IgG was determined spectrophotometrically. Next, using a CNBr-activated Sepharose 4B resin (GE Healthcare Life Sciences) on which ERD14 (1 mg) was immobilized according to the supplier's instructions, anti-ERD14 specific IgG were trapped and processed as described. Finally, the specificity of the anti-ERD14 IgG for its antigen was confirmed with ELISA prior to testing in functional/blocking assays (Supplementary Fig. 3). Mouse maintenance, care and experimental procedures complied with the European Convention for the Protection of Vertebrate Animals used for Experimental and Other Scientific Purposes guidelines (CETS n° 123) and were approved by the Ethical Committee for Animal Experiments (ECAE) at the Vrije Universiteit Brussel (Permit number: 14–220-04).

2.5. A. thaliana GSTF9 expression and purification

GSTF9 expression and purification was performed as described by Tossounian et al. [30] with minor changes. Briefly, the BL21(DE3) cells containing the gstf9-pDEST14 vector were lysed in the lysis buffer mentioned above and sonicated for 3 min (10 s on, 10 s off, 60% amplification). The collected supernatant after centrifugation (45 min, 20,000 xg, 4 °C) was incubated with 20 mM DTT for 30 min at 4 °C before loading onto a GSTrap FF 5 mL column (GE Healthcare Life Sciences). The column was washed with PBS and 1 mM DTT. GSTF9 was eluted in one step with the elution buffer (50 mM Tris pH 8.0, 0.1 M NaCl, 1 mM DTT and 10 mM GSH). After checking the purity on SDS-PAGE gel, samples were stored at −20 °C.

2.6. SDS-PAGE and western blot

The purified proteins were analyzed on 12.5% SDS-PAGE gel under reducing conditions, followed by PageBlue™ Protein Staining (Thermo Fisher Scientific). For western blot analysis, proteins were separated by SDS-PAGE under reducing condition, transferred onto polyvinylidene difluoride (PVDF) membranes (Bio-rad), probed with antibody against

ERD14, followed by incubation with HRP-conjugated anti-mouse IgG (Sigma-Aldrich). Bands were visualized by Pierce™ ECL western blotting substrate (Thermo Fisher Scientific) in a Biorad Chemidoc XRS System.

2.7. Quantification of hydrogen peroxide (H_2O_2) levels

The quantification of H_2O_2 concentrations in *Arabidopsis* WT, ERD14 OE and ERD14 KO plants transferred to FMS agar supplemented with or without 180 mM mannitol for three weeks, was performed as described by Velikova et al. [31]. The iodine (I_2) formation from the reaction of H_2O_2 in plant extracts and potassium iodide was measured in a BioTek Synergy plate reader at 390 nm. Three replicates of each condition and two measurements of each sample were performed. The H_2O_2 concentration was calculated from a H_2O_2 standard curve.

2.8. Histochemical detection of H_2O_2 accumulation

To visualize H_2O_2 accumulation in plant leaves, we performed an assay described in the method of Liu et al. (2015) [32]. Greenhouse plants were stopped watering for three days, then immersed into 1 g/L diaminobenzidine solution at pH 3.8 (Sigma-Aldrich), vacuum-infiltrated and kept in the solution at room temperature (RT) for 8 h. They were then washed with ethanol:lactic acid:glycerol (3:1:1 ratio), and photographed with Nikon G9 digital camera. Brown coloration of the leaves is proportional to H_2O_2 content.

2.9. Mass spectrometric analysis

ERD14 KO and WT plant seedlings were either treated or not with solid 100 mM mannitol for two weeks after which the proteome was analyzed. Three biological replicates with 10 seedlings each, were prepared for each condition. To make signal intensities (protein quantities) between different samples comparable, we took great care to handle them the same. The frozen material was crushed using pestle and mortar, and suspended in homogenization buffer. Cells were lysed by probe sonication and the proteins were precipitated using methanol:chloroform:water. The protein content of pellets was measured and the same amount of pellet in different samples was solubilized and cysteine residues were reduced with DTT and blocked with IAM, respectively, prior to overnight digestion with trypsin. The peptides were cleaned using Sampli-Q solid-phase extraction cartridges (Agilent) and eluted using 60% ACN, 0.1% TFA in dH_2O. The samples were completely dried under vacuum and stored at −20 °C.

The peptides were first loaded onto a trapping column (house-made, 100 μm I.D. × 20 mm, 5 μm beads C18 Reprosil-HD, Dr. Maisch, Germany) using loading solvent A (0.1% TFA in water/ACN, 98/2 (*v*/v)) and separated on an analytical column (house-made, 75 μm I.D. × 40 mm, 1.9 μm beads C18 Reprosil-HD, Dr. Maisch) using a 150 min non-linear gradient from 2% to 97% solvent B (0.1% formic acid in water/ACN, 20/80 (v/v)). Column temperature was kept constant at 50 °C (Sonation COControl).

The mass spectrometer was operated in data-dependent, positive ionization mode with the following MS1 parameters: resolution of 60,000, 375–1500 *m/z* scan range, AGC target of 3E6 ions, maximum ion time of 45 msec. The 16 most intense ions with a minimum charge of +2 and intensity of 1.3E4 were isolated within a 1.5 m/z window and fragmented in HCD mode (32% NCE). Ions accumulated for maximum 60 msec with a target AGC of 1E5.

Data analysis was performed with MaxQuant (version 1.5.3.8) using the Andromeda search engine with default settings during the main search including a 1% PSM, peptide and protein FDR, 20 and 4.5 ppm mass tolerance for MS1 and MS2 respectively. Spectra were searched against the UniProt/Swiss-Prot *A. thaliana* database (December 2016, 31,392 entries). Protease specificity was set to trypsin/P with a maximum of two missed cleavages. Carbamidomethylation of cysteine was set as a fixed modification and variable modifications were set to methionine oxidation and acetylation of protein N-termini. The following options were allowed: LFQ, second peptides and matching between runs. Further data analysis was performed with the Perseus software (version 1.5.2.4). Proteins only identified by site and reverse database hits were removed as well as potential contaminants. The replicate samples were grouped in 4 groups (ERD14 KO Ctrl, ERD14 KO Treated, WT Ctrl and WT Treated) and proteins with less than three valid values in at least one group were removed. Missing values were imputed from a normal distribution around the detection limit. For each two-sample *t*-test a permutation-based FDR of 0.01 with an S0 value of 0.1 was used for truncation with a total of 1000 randomizations.

The mass spectrometry proteomics data have been deposited to the Proteome Xchange Consortium via the PRIDE [1] partner repository with the dataset identifier PXD012239. The data can be accessed by this following account, Username: reviewer04733@ebi.ac.uk. Password: sxuBUtHV

2.10. Real-time quantitative PCR

Four-week-old plants were treated with liquid FMS medium supplemented with 180 mM mannitol for 6 h. RNA was isolated by Promega™ SV Total RNA Kit. Samples were then treated with DNase-I to rule out all genomic DNA contamination. cDNA was synthesized by the RevertAid H Minus First Strand cDNA Synthesis Kit (Thermo Fisher Scientific). The expression level of ERD14 and GSTF9 in transgenic lines was analyzed by qPCR with CFX96 Real-time PCR system (Biorad). Primers designed by Primer-Blast can be found in the Supplementary Table 1.

A GoTaq qPCR Master Mix (Promega) was prepared according to the supplier's manual. The PCR cycling conditions were as follows: 95 °C for 2 min, followed by 35 cycles of 95 °C for 30 s and 59 °C for 1 min. The melting curve was routinely measured after 35 cycles to verify primer specificity. The relative expression level was calculated by using the application tool of Biorad CFX Manager and GraphPad Prism7.

2.11. Hanging-drop glutaraldehyde cross-linking

Glutaraldehyde cross-linking studies were performed on 10 μM of final protein (GSTF9 or ERD14) concentration separately or in 1:1 ratio mixture. For ERD14, the reaction was repeated at higher concentrations (75 μM and 150 μM). Briefly, 48-well crystallization plates were filled with 120 μL of 25% glutaraldehyde (*v*/v) and 3 μL of 5 N HCl was added. 10 μL of each sample was placed on the cover slip. Samples were incubated at 25 °C for 15 min and analyzed on SDS-PAGE gel [33]. ERD14 was then detected by western-blotting with anti-ERD14 primary antibodies.

2.12. Microscale thermophoresis (MST) measurement

The Monolith® NT.115 instrument (Nano Temper) was used to study the interaction between ERD14 and GSTF9, or catalase. All assays were performed in PBS-T buffer (PBS, 10 mM $MgCl_2$, 0.05% Tween 20).

For the GSTF9 – ERD14 interaction assay, ERD14 was labeled with 100 μM Atto 647 NHS ester dye (Sigma Aldrich). ERD14 (50 μM) in PBS was added to the dye and incubated at RT for 30 min in darkness. The mixture was buffer exchanged with the Zeba™ desalting spin column (7 K MWCO - Thermo Fisher Scientific), to the reaction PBS-T buffer. In the assay, 500 nM Atto-647 labeled ERD14 was titrated with increasing GSTF9 concentrations (18 nM to 600 μM). A 16-step 2-fold dilution series of GSTF9 in PBS-T buffer was prepared, with a final volume of 10 μL in each reaction tube. Mixtures were loaded to 16 standard Monolith NT-115 capillaries. MST was carried out at 20% LED power and 40% MST power.

For the catalase – ERD14 interaction assay, the experiment was performed with labeled catalase. 40 μM Atto 647 NHS dye was added to

20 μM catalase (Sigma-Aldrich) in PBS buffer and the reaction mixture was incubated in the dark for 30 min, followed by a desalting step to PBS-T to remove non-reacted dye. In the assay, 400 nM Atto-647 labeled catalase was titrated with a 16-step 2-fold dilution series of ERD14 (120 μM to 3 μM) and measured in standard capillaries. The LED power and MST power were set at 20% and 50%, respectively. The K_D was obtained by plotting the initial fluorescence signal against the ligand concentration and calculated based on the formula of mass action law. NT Analysis software was used for analysis.

2.13. Effect of ERD14 on GSTF9 activity

The glutathione transferase assay was performed as described by Tossounian et al. [30]. The GSTF9 catalyzed conjugation of glutathione (GSH) onto 1-chloro-2,4-dinitrobenzene (CDNB) was measured at 340 nm using a spectrophotometric assay. To measure the influence of ERD14 on the glutathione transferase activity of GSTF9, 8 μM GSTF9 was incubated with ERD14 at molar ratios of 1:1,1:2,1:5, 1:10 and 1:15 at 25 °C for 1 h, and then 20 μL of the sample mixture was transferred to the assay mixture (200 μL) for the measurements. A reaction mixture containing ERD14 in the absence of GSTF9 was used as a control.

To evaluate the protection of GSTF9 by ERD14 against activity loss elicited by oxidation, reduced and oxidized GSTF9 activities were measured in the absence and presence of 10-times molar excess of ERD14. Oxidation of GSTF9 was performed as described by Jacques et al., 2015 [34]. For the oxidized sample, ERD14 was either pre-incubated with GSTF9 prior to oxidation for 5 min or added after oxidation right before measuring the activity. At least 2 independent replicates were measured for each condition. The progress curves were constructed in GraphPad Prism7.

2.14. Active-site titration of GSTF9

Before the assay, GSTF9 was reduced with 10 mM DTT for 30 min at RT and the samples were gel filtered using Superdex75 HR 10/30 size exclusion chromatography (SEC) column equilibrated in PBS. To determine the concentration of active enzyme molecules in the GSTF9 sample, an active-site titration experiment was performed on a stopped-flow instrument (Applied Photophysics), where the changes in absorbance at 340 nm were monitored. The pre-steady-state phase of the kinetics (burst) of the reaction was visualized and quantified. The first syringe contained 1 mL of GSTF9 and GSH in 250 mM MOPS pH 6.5, whereas the second syringe contained 1 mL of CDNB in the same buffer. Upon rapid mixing under high pressure, a clear burst was observed at 2 mM CDNB and 0.25 mM GSH. This condition was chosen for the active-site titration test of GSTF9 and ERD14. The product formed during the burst can be calculated using Eq. 1, in which Y intercept is the height of the burst of product formation observed (Absorbance at 340 nm, Au), $\varepsilon_{CDNB\text{-}GSH}$ is the molar extinction coefficient of CDNB-GSH conjugate at 340 nm (M^{-1} cm^{-1}) and ⌊ is the pathlength (cm). Eq. 1:

$$\text{Product formed} = \frac{\text{Y intercept}}{\varepsilon_{CDNB\text{-}GSH} \times \iota} \times 100.00 \quad (\mu M) \tag{1}$$

In the assay addressing the effect of ERD14 on GSTF9 activity, increasing GSTF9 concentrations (1 μM to 6 μM) were incubated with ERD14 at a molar ratio of 1:5 for 5 min prior to the measurement. In a typical enzymatic reaction, the progress curve has two phases, a pre-steady-state phase (burst), followed by a linear steady-state phase. The height of which (the magnitude of Y-intercept of extrapolated steady-state phase) represents the amount of product formed in the first round of catalytic reaction. Three independent replicates (Y-intercept value) were measured in each condition.

2.15. Catalase dehydration test and activity assay

Catalase (2 U) was treated in the absence and presence of 0.8 μM ERD14. The samples were then dehydrated overnight at RT in a vacuum chamber with silica gel. The same volume of MilliQ water as the evaporated buffer was added to rehydrate the samples 40 min prior to the measurement. Catalase activity was performed as described by Weydert and Cullen (2010) and measured based on H_2O_2 reduction at 25 °C in a BioTek Synergy plate reader at 240 nm.

2.16. Prediction of protein-protein interaction sites by RaptorX

RaptorX Complex Contact Prediction was used to predict the interaction sites of both ERD14 and GSTF9. The program takes two potentially interacting protein sequences into consideration and uses co-evolutionary information and ultra-deep learning techniques [35]. The results are shown in a heat map, in which darker regions mark the higher probability of contact for the given residues.

3. Results

3.1. ERD14 decreases the H_2O_2 levels in plants under osmotic stress

Osmotic stress causes the elevation of the level of H_2O_2 in plant cells [3]. To assess whether ERD14 has a role in controlling the H_2O_2 level under osmotic stress conditions, H_2O_2 was measured spectrophotometrically at 390 nm with potassium-iodide in the wild-type (WT), ERD14 knockout (KO), and ERD14 overexpressing (OE) *Arabidopsis* lines exposed to mannitol, which mimics osmotic stress in vitro. We present the H_2O_2 level in cells as a fresh weight (FW) ratio. This normalization is based on the fact that under osmotic conditions, stressed plants lose more water than non-stressed plants. The H_2O_2 level in the stressed plant cells is probably even more concentrated due to a lower water content than non-stressed plant cells. Under mannitol stress, the H_2O_2 levels in WT and ERD14 KO plants was significantly increased (Fig. 1A). Under non-stressed conditions, the H_2O_2 accumulation was similar for all three lines.

Moreover, the accumulation of H_2O_2 in ERD14 KO plants under water loss condition was histochemically confirmed (Fig. 1B). Using diaminobenzidine on dehydrated leaves of WT, ERD14 OE and ERD14 KO plants after three days of water deprivation, the accumulation of H_2O_2 was clearly observed (Fig. 1B), while under normal (non-stressed) conditions, the presence or absence of ERD14 did not affect the H_2O_2 levels. Under dehydration conditions, the H_2O_2 level of WT plants increased notably, and even further increased in the ERD14 KO plants. On the other hand, there was only a minor increase of H_2O_2 in the leaves of ERD14 OE plants (Fig. 1B). In the ERD14 OE line, the difference in H_2O_2 level was less pronounced, indicating that ERD14 is directly involved in decreasing the level of H_2O_2 in plants under dehydration conditions.

3.2. Osmotic stress increases the expression of GST enzymes

To explain the observed decrease of H_2O_2, we decided to investigate the upregulation of specific redox enzymes in the presence and absence of ERD14. Therefore, we compared the proteome of WT and ERD14 KO plants under mannitol stress with non-stressed plants.

Protein extracts of *Arabidopsis* seedlings subjected to mannitol stress were collected, purified, and denatured before being digested with a trypsin/LysC endoprotease mixture. The resulting peptide mixtures were analyzed by mass spectrometry (MS) and quantified using MS1 label-free quantification. A two-sample *t*-test was used to compare the change in protein levels as an effect of mannitol treatment in the ERD14 KO and WT lines individually (PRIDE accession number: PXD012239).

Among the redox enzymes present in the MS data (Table 1, Supplementary Table 2), we decided to follow the GST Phi proteins (GSTFs), because this group of proteins contains members, which are affected in the absence of ERD14 under osmotic stress (Supplementary Table 2). Moreover, they are redox enzymes with an important role in

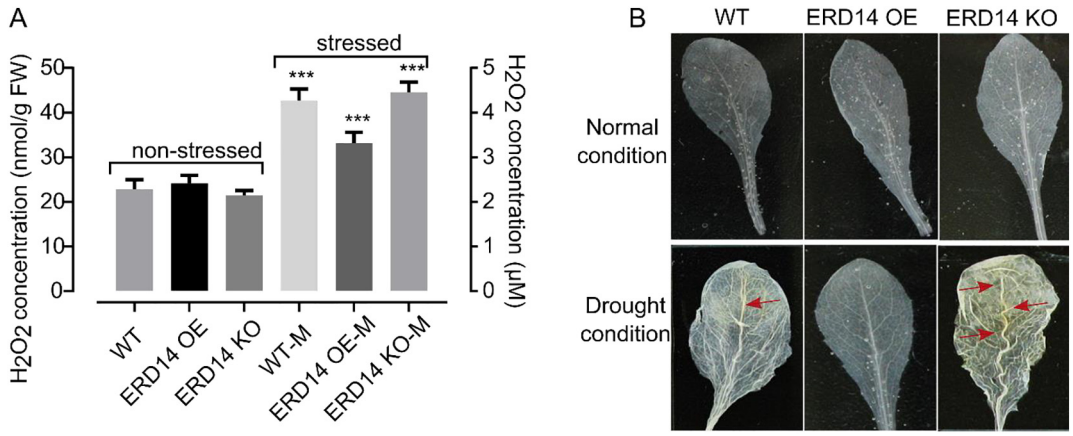

Fig. 1. Osmotic stress increases the H_2O_2 levels in *A. thaliana* plants. (A) Hydrogen peroxide accumulates in plants under osmotic stress. The bar chart shows the H_2O_2 concentration (nmol/g FW or µM) in extracts obtained from WT, ERD14 KO and OE plants kept without stress or exposed to mannitol-induced stress. FW refers to fresh weight of plants. The concentrations obtained spectrophotometrically at 390 nm with potassium-iodide show that plants subjected to 180 mM mannitol for 3 weeks accumulate higher levels of H_2O_2 compared to non-stressed plants. All data represent the mean +/− standard deviation of three replicates. Statistical analysis was performed by one-way ANOVA with multiple comparisons, which revealed significant differences between different group of samples (stressed and non-stressed plants; stressed WT and stressed ERD14 OE; stressed WT and stressed ERD14 KO, stressed ERD14 KO and stressed ERD14 OE), indicated in the figure by asterisk *** $p < 0.0001$. (B) Hydrogen peroxide accumulates in ERD14 KO plant leaves exposed to drought stress. Four-week old *A. thaliana* WT, ERD14 OE and ERD14 KO plants were subjected to drought stress and the H_2O_2 level was visualized by diaminobenzidine staining. The regions with arrows indicate H_2O_2 accumulation.

plant survival under different stress conditions [36] and research on their oxidative stress response is rather limited. We found that WT plants under mannitol stress have increased levels of GSTFs (GSTF2 and GSTF6). Under stress and in the absence of ERD14, the protein levels of other GST Phi members (GSTF2, GSTF6, GSTF7, GSTF8, GSTF9 and GSTF10) increased significantly (Table 1), indicating a role for GSTFs in removing H_2O_2 under osmotic stress in the absence of ERD14, suggesting a possible compensatory mechanism for the loss of ERD14.

3.3. ERD14 has no impact on the transcript level of GSTF9 under osmotic stress

These results raised questions on how ERD14 could affect redox enzymes under osmotic stress. To get further insights, we decided to focus on one protein of the GSTF family, GSTF9, which protein level increased two-fold under stress (Table 1). Notably, the transcript of GSTF9 was upregulated under drought stress in rapeseed *(Brassica napus L)* [37] and silencing of *At*GSTF9 altered the oxidative stress tolerance of *A. thaliana* [38]. Further, GSTF9 plays an important role in maintaining the cellular redox homeostasis under drought stress.

With cDNA isolated from *Arabidopsis* plants (WT, ERD14 OE, and ERD14 KO) exposed to 180 mM mannitol-stress for 6 h, we quantified the transcript level of ERD14 and GSTF9. We observed that WT plants under mannitol stress showed an increase of the transcript level of ERD14 and GSTF9 compared to the non-stressed plants (Fig. 2). In ERD14 OE and ERD14 KO plants, the transcript level of GSTF9 showed a similar increase as for WT plants, and this is independent of the applied mannitol stress.

This result clearly confirmed our proteomic data (Table 1), and indicates that ERD14 might impact the protein activity of GSTF9, but not its transcription.

3.4. ERD14 interacts directly with GSTF9

To understand whether the stress tolerance of ERD14 OE plants is due to a direct interaction of ERD14 on GSTF9, we decided to investigate whether recombinantly expressed and purified ERD14 and GSTF9 proteins can physically interact with each other. First, we evaluated protein band shifts after crosslinking with a Lys-reactive crosslinker, glutaraldehyde, on an SDS-PAGE gel and on western blot (Fig. 3). On the SDS-PAGE gel, homo-dimeric GSTF9 [39] migrates as a dimeric band around 48 kDa (Fig. 3A – lane 2), while ERD14 appears as a diffuse band after 15 min incubation with the crosslinker (Figs. 3A and B - lane 6). This result suggests a heterogeneous intermolecular cross-linking within monomeric ERD14. When GSTF9 was incubated with ERD14, two higher-MW bands were observed around 50 kDa and

Table 1
Mass spectrometric analysis shows an increase of the levels of GST Phi proteins under osmotic stress. This table shows proteomic data of WT and ERD14 KO plants treated with 100 mM mannitol for 2 weeks. The differences of protein levels under stress conditions and in untreated plants (log_2 ratio) is assessed by two-sample *t*-testing. Proteins are indicated by their UniProt ID and genome annotation in the *Arabidopsis* Information Resource (TAIR). Data analysis was performed with MaxQuant using Andromeda search engine with default search settings including a false discovery rate set at 1% on both the peptide and protein level.

Protein	UniProt ID	TAIR10	WT treated vs WT untreated		KO treated vs KO untreated	
			Log_2 ratio	Significant	Log_2 ratio	Significant
GSTF2	P46422	At4g02520	1.76	+	2.40	+
GSTF3	Q9SLM6	At2g02930	1.31		1.74	
GSTF6	P42760	At1g02930	2.95	+	4.26	+
GSTF7	Q9SRY5	At1g02920	3.69		5.35	+
GSTF8	Q96266	At2g47730	0.33		1.95	+
GSTF9	O80852	At2g30860	1.05		1.81	+
GSTF10	P42761	At2g30870	0.81		2.07	+
GSTF12	Q9FE46	At5g17220	2.16			

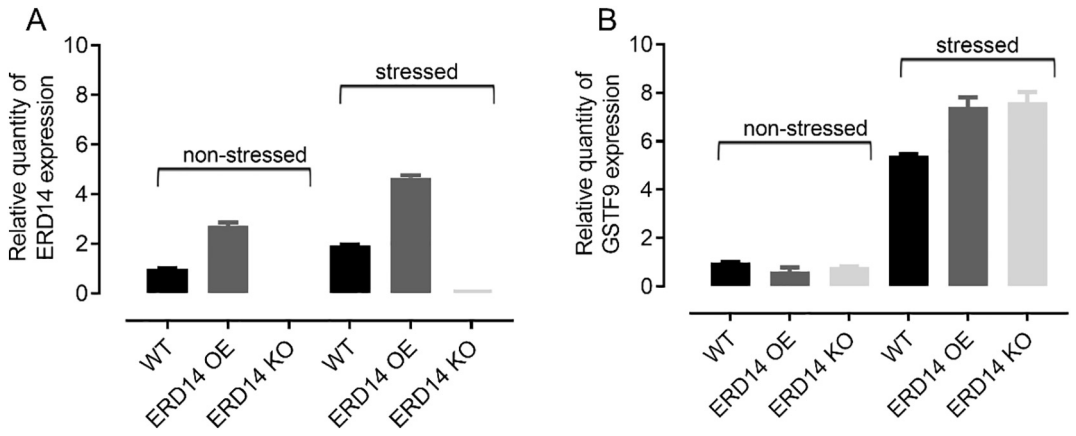

Fig. 2. Osmotic stress causes an increase of the ERD14 and GSTF9 expression levels. The bar graphs show the RT-PCR relative quantity of (A) ERD14 and (B) GSTF9 expression after 6 h mannitol stress or non-stress conditions in WT, ERD14 OE and KO plants. (A) Under mannitol stress, compared to non-stressed WT, ERD14 is expressed 2 times more in WT and 4 times more in ERD14 OE lines. (B) GSTF9 is expressed 5 times more in WT and 7 times more in ERD14 OE and ERD14 KO plants subjected to mannitol stress, compared to non-stressed controls. Data represent means of ($n = 2$) independent experiments.

100 kDa. As the migration position of the bands in Fig. 3, lane 2 and 4 are very similar, we produced a specific anti-ERD14 antibody from mouse for western blot analysis. The western blot shows that ERD14 interacts with GSTF9 (Fig. 3B – lane 4). The signal of the ERD14 band was stronger in the western blot than the SDS-PAGE gel, because ERD14 is enriched in disorder-promoting amino acids (Gly, Ser, Lys, Glu, and Pro) and depleted in the order-promoting amino acids Trp and Cys. This compositional bias leads to a low molar extinction coefficient at 280 nm and a weak binding to the Coomassie blue dye [40]. Interestingly, when we performed cross-linking at higher ERD14 concentrations (75 μM and 150 μM ERD14), we noticed the appearance of higher-MW bands at 50 kDa, 70 kDa and 200 kDa, indicating a tendency of ERD14 for oligomerization at higher concentrations (Supplementary Fig. 1 - lanes 5 & 6 (75 μM) and lanes 8 & 9 (150 μM)) while at low concentration of ERD14 (10 μM), the ERD14 oligomerization was not easily detected with slightly weaker signal at 35 kDa at 15 min incubation (Figs. 3A and B - lane 6). This result showed that ERD14 physically interacts with GSTF9, which might have a possible impact on the enzyme activity.

3.5. ERD14 interacts with GSTF9 with a K_D of 25 μM

Next, we decided to determine the affinity between ERD14 and GSTF9 and their potential interaction sites. To determine the dissociation constant (K_D) of the ERD14-GSTF9 complex, microscale

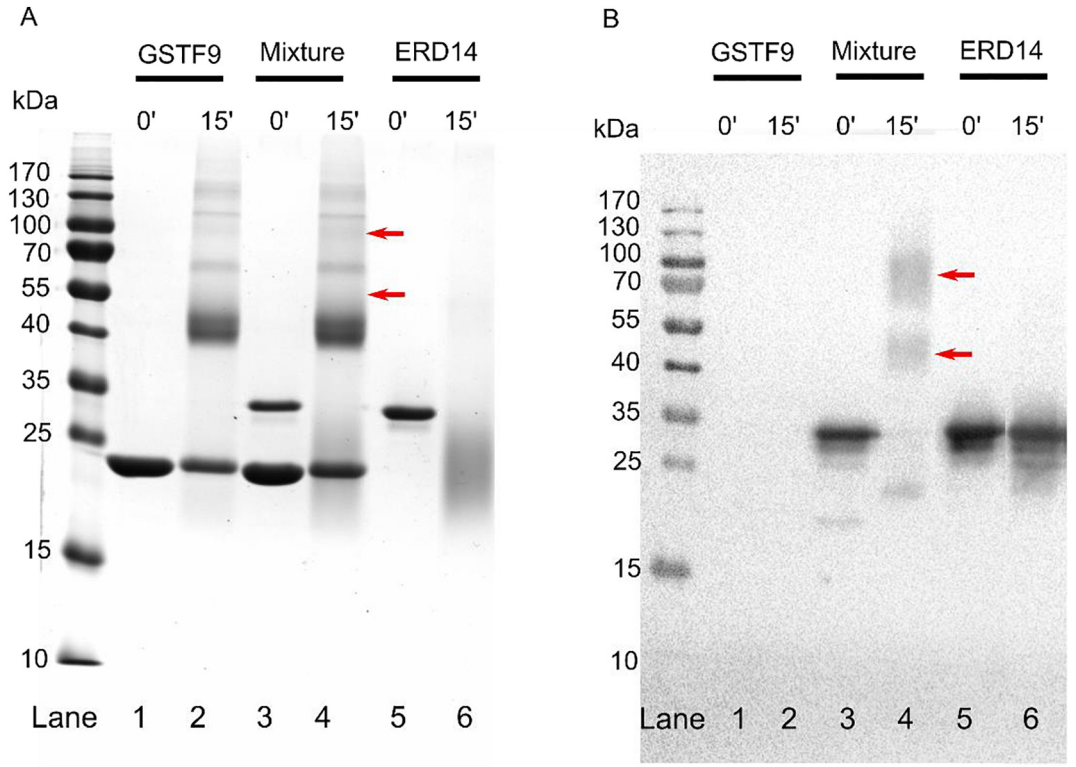

Fig. 3. Interaction between ERD14 and GSTF9 as observed by glutaraldehyde cross-linking. (A) A SDS-PAGE gel and (B) an anti-ERD14 western blot are shown. Ten micromolar of final protein concentration of GSTF9 (lanes 1 and 2), ERD14 and GSTF9 (1:1 molar ratio) (lanes 3 and 4) or ERD14 (lanes 6 and 7) were incubated for 15 min with glutaraldehyde (25%) in a hanging-drop format. The samples were run on 15% SDS-PAGE gel or transferred to a PVDF membrane for western blotting. Higher molecular weight bands are observed at about 50 kDa and 100 kDa (red arrows), which are the products of cross-linking between GSTF9 and ERD14.

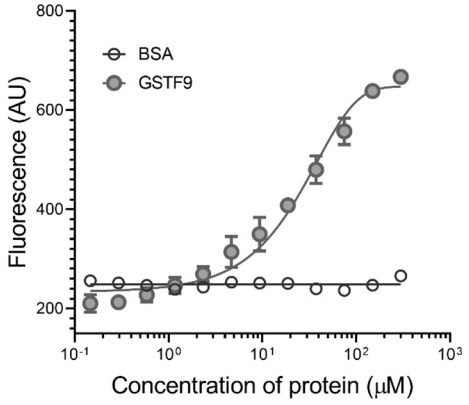

Fig. 4. ERD14 interacts with GSTF9. The baseline fluorescent signal of Atto 647-labeled ERD14 plotted against GSTF9 or BSA concentration (μM) obtained by using microscale thermophoresis (MST) is shown. A K_D value of 25.1 ± 1.2 μM was calculated for the ERD14 and GSTF9 interaction and obtained by fitting with the formula of mass action law. No interaction was shown for ERD14 and BSA. All data represent the mean ± standard deviation of three replicates. The standard deviations of BSA samples are too small to be shown.

thermophoresis (MST) was used. In this experiment, ERD14 was labeled with the Atto 647 HNS ester dye, which reacts with primary amines of proteins. MST traces showed that the ligand – GSTF9 caused a decrease in baseline fluorescence due to the binding of ligand in close vicinity to the dye. Therefore, the baseline data was used rather than the temperature jump or thermophoresis data to assess molecular binding [41]. Data showed a weak affinity with a K_D of 25.1 ± 1.2 μM (Fig. 4). This affinity is of particular interest, because common dissociation constants for protein-protein interactions of globular proteins tend to be in the nM range [42], whereas chaperones engage in weak and transient interactions with their targets [43] with significantly higher K_Ds.

3.6. ERD14 activates GSTF9 and protects against oxidation

Osmotic stress increases the level of H_2O_2, which leads to the activation of several anti-oxidant enzymes, but it can also damage biomolecules [44]. Due to its direct interaction with GSTF9, we decided to investigate the effect of ERD14 on GSTF9 under oxidative conditions. To this end, we measured the glutathione transferase activity of GSTF9 under steady-state conditions in the absence and in the presence of varying molar ratios of ERD14 (Fig. 5A). When incubated at a 1:5, 1:10 or 1:15 GSTF9:ERD14 ratio, an increase of the enzyme activity of GSTF9 was observed (Fig. 5A), which indicated a possible chaperone-like activity of ERD14. Interestingly, oligomerization of ERD14 was also observed at higher concentrations, which occur at a ratio 1:10 (80 μM of ERD14), which might be indicative of the way ERD14 interacts (Supplementary Fig. 2).

To determine whether ERD14 can protect GSTF9 under oxidizing conditions, we pre-incubated the enzyme with 0.03% H_2O_2 for 135 min before measuring its activity (Fig. 5B). In agreement with previous reports [30], 50% of the transferase activity is lost upon oxidation under these conditions. However, if we incubated GSTF9 with ERD14 for 5 min prior to oxidation ([GSTF9 + ERD14] + H_2O_2]), the oxidized GSTF9 activity only decreases 16% compared to the reduced control. This result indicates an 84% protection of the enzymatic activity by ERD14 against oxidative damage. To address whether ERD14 can activate oxidized GSTF9, we first oxidized GSTF9, and then incubated with ERD14 for 10 min before measuring enzyme activity ([GSTF9 + H_2O_2] + ERD14]). In this case, activation was 27%, showing that ERD14 can re-activate GSTF9 after it has been oxidized. These results suggest that ERD14 can increase the GSTF9 enzyme activity and also protect the enzyme from losing its activity upon oxidation, i.e. the IDP chaperone exerts a combined effect under oxidizing conditions (Fig. 5B).

3.7. ERD14 activates inactive GSTF9 molecules

To address whether ERD14 is able to increase the activity of already active enzyme molecules, or, rather, reactivate inactive GSTF9 molecules, we carried out pre-steady-state stopped-flow active-site titration experiments (Fig. 6). We found that only 21% of GSTF9 molecules are active in the absence of ERD14 (Fig. 6A), whereas if GSTF9 is pre-incubated with a 5-fold molar excess of ERD14 for 5 min at 25 °C, the ratio of active enzyme molecules increases to 41% (Fig. 6B). This indicates that ERD14 has the potency to turn inactive enzyme molecules into active ones, whereas it cannot increase the specific activity of already active molecules, as apparent from the steady-state part of the reaction showing the exact same level of activity with and without ERD14.

3.8. ERD14 protects catalase under de-hydration conditions

To see whether similar effects of ERD14 can be observed for other redox enzymes, we moved on to test a well-known anti-oxidant enzyme – catalase. Catalases participate in the detoxification of H_2O_2 in plants exposed to several abiotic stress conditions [45,46]. Therefore, it has been chosen as a popular target and was intensively studied in oxidative stress response [46], especially for some dehydrins [16,47], however, it has not been shown to be a binding partner and/or a client of ERD14. With MST, a K_D of 126 ± 13.3 nM for the complex formation between ERD14 and catalase was obtained (Fig. 7A). We next tested whether ERD14 activates the enzymatic activity of catalase in a dehydration assay (Fig. 7B). Catalase was dehydrated overnight in the absence or

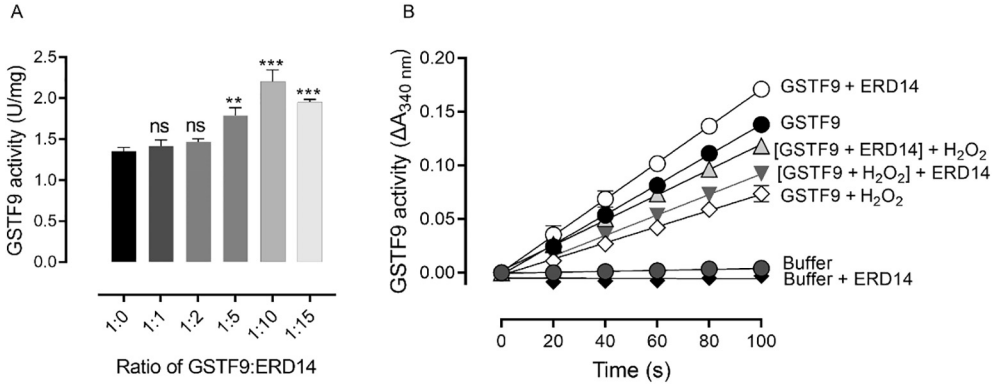

Fig. 5. ERD14 activates GSTF9 and protects against oxidation. (A) Samples with different ratios of GSTF9-ERD14 were incubated for 1 h at room temperature and the glutathione transferase activity was compared. In the presence of ERD14 with different excess ratio, the GSTF9 transferase activity has increased by 30% (1:5 ratio), 80% (1:10 ratio) and 45% (1:15 ratio). (B) Progress curves monitoring the increase of A_{340} in function of time. When oxidized (GSTF9 + H_2O_2), the transferase activity of GSTF9 decreases by 50%. In the presence of 10-times excess of ERD14, the GSTF9 activity decreases by 16% compared with reduced sample. ERD14 protects the GSTF9 activity when incubated with GSTF9 prior to the exposure to H_2O_2 stress condition ((GSTF9 + ERD14) + H_2O_2). But when GSTF9 is first exposed to oxidative stress and then incubated with ERD14 ([GSTF9 + H_2O_2] + ERD14), the activation is 27%. All data represent the mean ± standard deviation of three replicates.

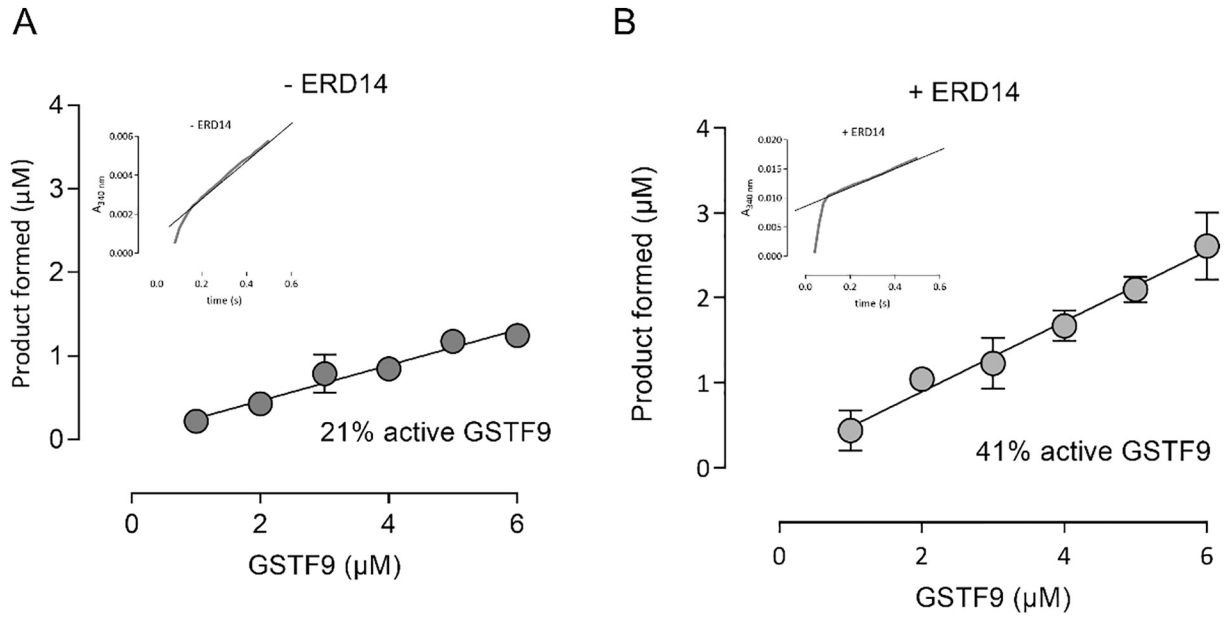

Fig. 6. ERD14 activates inactive GSTF9 molecules. Active site titration of GSTF9 was carried out by stopped-flow measurements by comparing the pre-steady state burst of GSTF9 in the (A) absence or (B) presence of ERD14. GSTF9 was pre-incubated for 5 min at 25 °C in the absence or presence of 5-fold molar excess of ERD14, and formation of the product was followed in function of time within the first second of the reaction (inserts). The product formation was plotted in the function of GSTF9 concentration and the percent activity of GSTF9 was determined using linear regression. In the presence of ERD14, the percentage of active GSTF9 enzymes increases from (A) 21% to (B) 41%.

presence of ERD14 in the vacuum chamber with silica-gel and subsequently resolubilized with water for 40 min before measuring its activity. In the presence of ERD14, dehydrated catalase activity was 40% higher than in its absence (Fig. 7B), which indicate that ERD14 can also protect this enzyme.

4. Discussion

At normal physiological levels, H_2O_2 has a signaling role in plant development and growth [48], whereas under osmotic stress, its cellular levels increase [49] and H_2O_2 becomes a messenger molecule that leads to the up-regulation of stress-resistance genes, redox enzymes, and reducing pathways. By exposing *Arabidopsis* plants to osmotic stress, we observed an increase of the levels of H_2O_2 (Fig. 1), which also has been shown for wheat and maize under drought stress [49,50].

In this study, we aimed to understand the role of ERD14 in the oxidative stress response under osmotic stress. ERD14 mediates early responses to dehydration and is an effective chaperone protecting a broad range of partner proteins in vitro [14]. As dehydrins impart stress tolerance when expressed in various hosts [16], we hypothesized that ERD14 may play a direct role in the oxidative response under osmotic stress, which has been shown for its paralogue ERD10 under drought and cold stress [14,27]. ERD10 also falls in the K_2S class of dehydrins [23] and shows about 70% sequence identity to ERD10.

By exposing *Arabidopsis* ERD14 KO and ERD14 OE plants to mannitol stress, we monitored H_2O_2 formation. A decrease of the H_2O_2 levels was observed in ERD14 OE plants under stress, while ERD14 KO plants showed similar H_2O_2 levels as WT plants (Fig. 1). This suggests that ERD14 may play a role in redox homeostasis during osmotic stress response. To connect ERD14 with other stress-response proteins, we performed a proteomic analysis on WT and ERD14 KO plants under non-stress and mannitol-induced osmotic stress, and observed a significant increase in the protein levels of GST Phi enzymes (Table 1) in ERD14 KO plants.

Plant GST enzymes are known to be involved in xenobiotic detoxification and in plant response to biotic and abiotic stresses [51–53]. GSTF9 functions as a glutathione transferase and a weak glutathione-dependent peroxidase, that scavenges peroxides generated during oxidative stress [30,54]. Therefore, we decided to study here the effect of ERD14 on the stability and activity of GSTF9.

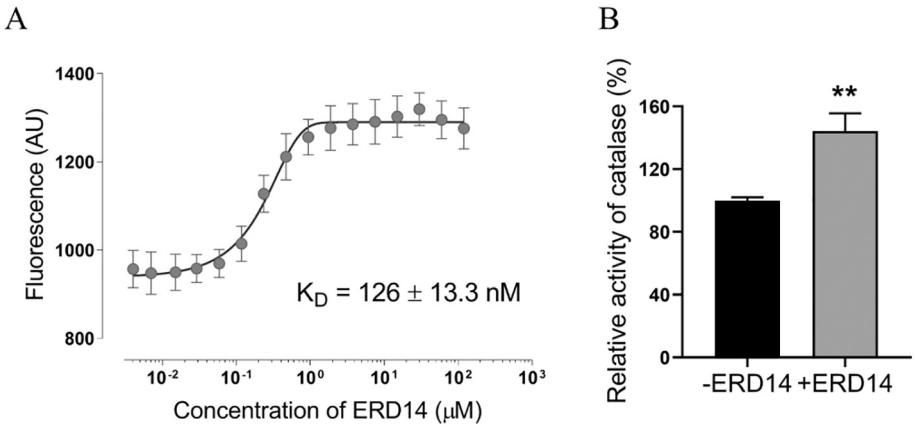

Fig. 7. ERD14 interacts with catalase. (A) A 16-point two-fold serial dilution concentration response curve of ERD14 (from 120 μM to 3 nM) was measured by following the florescence of 400 nM Atto-647-labeled catalase (CAT) in MST. The fluorescent signal was plotted in the function of ERD14 concentration and fitted by the law of mass action formula. A K_D value of 126 ± 13.3 nM was determined. All data represent the mean ± standard deviation of three replicates. (B) ERD14 activates dehydrated catalase under dehydration conditions. Data are reported as mean ± SD, n = 3 replicates per condition. Statistical analysis was performed by t-test, which revealed significant differences between sample with and without the addition of ERD14, indicated in the figure by asterisk ** p < 0.001.

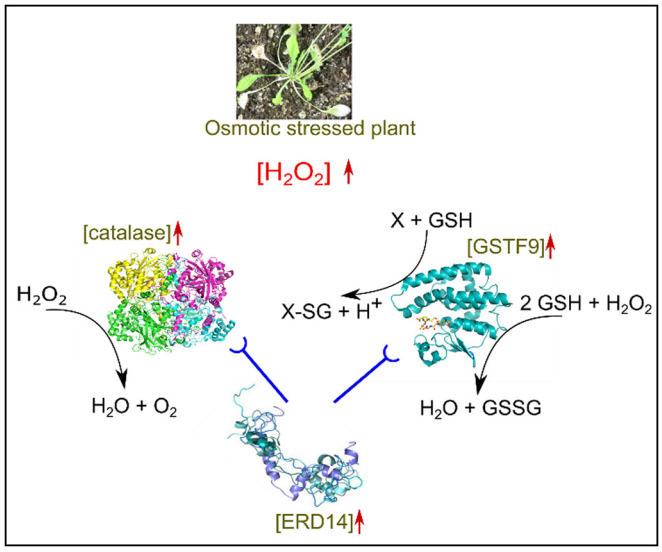

Fig. 8. Proposed ERD14 mechanism for the protection of plants under osmotic stress. Possible pathways by which ERD14 can mitigate the adverse effects of dehydration and oxidative stress are shown. The red arrows indicate increase, whereas blue symbols indicate protection through interaction. The structures of GSTF9 (PDB 6F05), bovine liver catalase (PDB 1TGU), and ERD14 (an ensemble of an IDP) [69] are shown. Under osmotic stress, high H_2O_2 concentrations negatively affect plant growth and development. One of the responsive ways is the production of enzymes to detoxify, such as catalase and GSTF9. Catalase converts H_2O_2 to water. GSTF9 reduces H_2O_2 and transfers GSH to xenobiotics. ERD14 is upregulated and acts as a chaperone, protecting redox enzymes to increase stress tolerance.

Although we observed an increase in the protein level of GSTFs under osmotic stress in ERD14 KO plants (Table 1), accumulation of H_2O_2 was still observed in these plants under mannitol stress (Fig. 1). Under osmotic stress, it has been reported that GSTF9 KO plants accumulate H_2O_2 [54], indicating that GSTF9 expression is linked to the levels of H_2O_2. However, both ERD14 OE and KO plants showed similar increase in GSTF9 expression, which indicates an unclear correlation between transcript levels of GSTF9 and the H_2O_2 concentration. This was unexpected, and the results obtained from the proteomic study and transcript evaluation could not clarify the role of ERD14 under osmotic stress. To explain this observation, we studied the ERD14 - GSTF9 interaction and the impact of ERD14 on the activity of GSTF9.

Interestingly, both GSTF9 and catalase directly interact with ERD14, which, due to the chaperone activity of ERD14, physically connects this IDP chaperone with redox enzymes. Whereas traditional chaperones function by two broad mechanisms [55]. Holdases seclude the structurally compromised client protein (in a way ensuring conditions of “infinite” dilution) and provide an extended time window for their folding to occur, without aggregation. “Foldases”, on the other hand, use ATP energy to conduct an iterative series of release and re-binding reactions to nurture the client toward its native structural and functional state. Often, the two mechanisms cannot be separated, and well-studied chaperones like GroEL/GroES or the Hsp90 family, harness both mechanisms. IDP chaperones cannot use ATP as energy source, and are thought to operate primarily as holdases, by space filling/molecular shield [56] or entropy transfer [24] mechanisms. In all the cases, chaperones engage in weak and transient partner binding specific to the misfolded state of the client.

In agreement, the K_D of the ERD14 - GSTF9 interaction (~25 μM) (Fig. 4) is higher than that of the ERD14-catalase interaction (0.13 μM) (Fig. 7A), but it is still in general agreement with the low affinity of chaperones for their target proteins. For example, in the case of IDP chromatin protein NUPR1 (Nuclear Protein 1), it interacts with the C-terminal region of RING1B (Ring finger protein 1) with an affinity in the micromolar range (~10 μM). Interactions with a K_D in the micromolar to millimolar range are emerging as important for signaling, regulation, and stress adaptation [57–59]. The weak but specific interaction of ERD14 with its targets could provide an important redox regulatory mechanism in cells [60,61].

As suggested, dehydrins consist of several conserved lysine-rich K-segments, which mediate protein-protein interactions [23] and give dehydrins a protein protection potential under oxidative stress conditions [20]. As ERD14 contains several K-segments (Supplementary Fig. 2A) [14], these regions are likely candidates for the interaction of ERD14 with GSTF9. Bioinformatic predictions suggested that this might be the case (Supplementary Fig. 2B). The K-segments of ERD14 are rich in Pro and Ala instead of Gly, and they also contain a high percentage of acidic residues [26,62]. This unique amino acid composition could stimulate binding specifically to GSTF9, but only with a relatively low affinity (Supplementary Fig. 2).

Homodimeric GSTF9 has an N-terminal thioredoxin-like domain, which contains the glutathione-binding site (G-site), and an alpha-helical domain on its C-terminal side, where hydrophobic substrates bind (H-site). The H-site contains several aliphatic (Ala, Ile, Val and Pro) and aromatic [13] residues, which become more flexible under oxidative stress [30]. Therefore, the interaction between GSTF9 and ERD14 could possibly lead to stabilization of the flexible H-site, which could explain the reactivation of inactive GSTF9 molecules (Fig. 6).

These observations directly link ERD14 to the osmotic stress response of *A. thaliana*. Our results showed that an IDP chaperone interacts with GSTF9 and catalase, and more importantly, ERD14 activates both redox enzymes. Because catalase and ERD14 share the same subcellular localization, such as cytoplasmic, peroxisomal and mitochondrial [63–66], whereas H_2O_2 can also be produced in chloroplast [67], peroxisomes [64] and also mitochondria [68], the effects of ERD14 on the redox enzymes in stress response can be generalized, as shown in Fig. 8. With the observed activation effects of ERD14, thus, additional regulatory layer represented by IDP dehydrins fine-tunes the plant protection mechanism against osmotic stress.

Declaration of Competing Interest

None.

Acknowledgments

We thank Karolien Van Belle for technical support and Leonardo Astolfi Rosado for the discussions.

This work was supported by (i) Vlaams Instituut voor Biotechnologie (VIB), (ii) Vietnamese Government Scholarship (911) granted to PNN (iii) FWO PhD fellowship granted to MAT, (iv the Strategic Research Programme (SRP34) of the VUB granted to JM, (v) the Research Foundation-Flanders (Excellence of Science project no. 30829584) to D.V. and J.M, (vi) the G0D7914N to J.M, (vii) the Odysseus grant (G.0029.12) to P.T., (viii) the Strategic Research Program (SRP3 and SRP47) of the VUB to B.S. and (ix) OTKA grants K124670 and K131702 from the Hungarian Scientific Research Fund to P.T. The funders had no role in study design, data collection and analysis, decision to publish, or preparation of the manuscript.

Appendix A. Supplementary data

Supplementary data to this article can be found online at https://doi.org/10.1016/j.bbagen.2019.129506.

References

[1] G. Noctor, A. Mhamdi, C.H. Foyer, The roles of reactive oxygen metabolism in drought: not so cut and dried, Plant Physiol. 164 (4) (2014) 1636–1648.
[2] K. Ben Rejeb, D. Lefebvre-De Vos, I. Le Disquet, A.S. Leprince, M. Bordenave,

R. Maldiney, A. Jdey, C. Abdelly, A. Savouré, Hydrogen peroxide produced by Nadph oxidases increases Proline accumulation during salt or Mannitol stress in *Arabidopsis Thaliana*, New Phytol. 208 (4) (2015) 1138–1148.
[3] G. Miller, N. Suzuki, S. Ciftci-Yilmaz, R. Mittler, Reactive oxygen species homeostasis and signalling during drought and salinity stresses, Plant Cell Environ. 33 (4) (2010) 453–467.
[4] S. Jang, J.A. Imlay, Micromolar intracellular hydrogen peroxide disrupts metabolism by damaging iron-Sulfur enzymes, J. Biol. Chem. 282 (2) (2007) 929–937.
[5] M.B. Arnao, M. Acosta, J.A. Del Río, F. García-Cánovas, Inactivation of peroxidase by hydrogen peroxide and its protection by a reductant agent, Biochim. Biophys. Acta 1038 (1) (1990) 85–89.
[6] E. Lamalakshmi Devi, S. Kumar, T. Basanta Singh, S.K. Sharma, A. Beemrote, C.P. Devi, S.K. Chongtham, C.H. Singh, R.A. Yumlembam, A. Haribhushan, N. Prakash, S.H. Wani, Adaptation strategies and defence mechanisms of plants during environmental stress, in: M. Ghorbanpour, A. Varma (Eds.), Medicinal Plants and Environmental Challenges, Springer International Publishing, Cham, 2017, pp. 359–413.
[7] R. Mittler, Oxidative stress, antioxidants and stress tolerance, Trends Plant Sci. 7 (9) (2002) 405–410.
[8] A. Ramachandra Reddy, K.V. Chaitanya, M. Vivekanandan, Drought-induced responses of photosynthesis and antioxidant metabolism in higher plants, J. Plant Physiol. 161 (11) (2004) 1189–1202.
[9] M. Hundertmark, D.K. Hincha, Lea (Late embryogenesis abundant) proteins and their encoding genes in *Arabidopsis Thaliana*, BMC Genomics 9 (118) (2008), https://doi.org/10.1186/1471-2164-9-118.
[10] M. Battaglia, Y. Olvera-Carrillo, A. Garciarrubio, F. Campos, A.A. Covarrubias, The enigmatic Lea proteins and other Hydrophilins, Plant Physiol. 148 (1) (2008) 6–24.
[11] T.J. Close, Dehydrins: emergence of a biochemical role of a family of plant dehydration proteins, Physiol. Plant. 97 (4) (1996) 795–803.
[12] J. Danyluk, A. Perron, M. Houde, A. Limin, B. Fowler, N. Benhamou, F. Sarhan, Accumulation of an acidic Dehydrin in the vicinity of the plasma membrane during cold acclimation of wheat, Plant Cell 10 (4) (1998) 623–638.
[13] M.K. Alsheikh, B.J. Heyen, S.K. Randall, Ion binding properties of the Dehydrin Erd14 are dependent upon phosphorylation, J. Biol. Chem. 278 (42) (2003) 40882–40889.
[14] D. Kovacs, E. Kalmar, Z. Torok, P. Tompa, Chaperone activity of Erd10 and Erd14, two disordered stress-related plant proteins, Plant Physiol. 147 (1) (2008) 381–390.
[15] M. Nylander, J. Svensson, E.T. Palva, B.V. Welin, Stress-induced accumulation and tissue-specific localization of Dehydrins in *Arabidopsis Thaliana*, Plant Mol. Biol. 45 (3) (2001) 263–279.
[16] T. Rorat, Plant Dehydrins-tissue location, structure and function, Cell. Mol. Biol. Lett. 11 (4) (2006) 536–556.
[17] S. Hughes, S.P. Graether, Cryoprotective mechanism of a small intrinsically disordered Dehydrin protein, Protein Sci. 20 (1) (2011) 42–50.
[18] I. Yruela, B. Contreras-Moreira, Protein disorder in plants: a view from the chloroplast, BMC Plant Biol. 12 (165) (2012), https://doi.org/10.1186/1471-2229-12-165.
[19] R. Allagulova Ch, F.R. Gimalov, F.M. Shakirova, V.A. Vakhitov, The plant Dehydrins: structure and putative functions, Biochemistry. Biokhimiia 68 (9) (2003) 945–951.
[20] Y. Liu, L. Wang, T. Zhang, X. Yang, D. Li, Functional characterization of Ks-type Dehydrin Zmdhn13 and its related conserved domains under oxidative stress, Sci. Rep. 7 (1) (2017) 1–10.
[21] M. Drira, W. Saibi, F. Brini, A. Gargouri, K. Masmoudi, M. Hanin, The K-segments of the wheat Dehydrin Dhn-5 are essential for the protection of lactate dehydrogenase and Beta-Glucosidase activities in vitro, Mol. Biotechnol. 54 (2) (2013) 643–650.
[22] M.C. Koag, S. Wilkens, R.D. Fenton, J. Resnik, E. Vo, T.J. Close, The K-segment of maize Dhn1 mediates binding to anionic phospholipid vesicles and concomitant structural changes, Plant Physiol. 150 (3) (2009) 1503–1514.
[23] S.P. Graether, K.F. Boddington, Disorder and function: a review of the Dehydrin protein family, Front. Plant Sci. 5 (October) (2014) 1–12.
[24] P. Tompa, P. Csermely, The role of structural disorder in the function of Rna and protein chaperones, FASEB J. 18 (11) (2004) 1169–1175.
[25] B.S. Ágoston, D. Kovács, P. Tompa, A. Perczel, Full backbone assignment and dynamics of the intrinsically disordered Dehydrin Erd14, Biomol. Nmr Assign. 5 (2) (2011) 189–193.
[26] T. Kiyosue, K. Yamaguchi Shinozaki, K. Shinozaki, Characterization of two Cdnas (Erd10 and Erd14) corresponding to genes that respond rapidly to dehydration stress in *Arabidopsis Thaliana*, Plant Cell Physiol. 35 (2) (1994) 225–231.
[27] S.Y. Kim, K.H. Nam, Physiological roles of Erd10 in abiotic stresses and seed germination of *Arabidopsis*, Plant Cell Rep. 29 (2) (2010) 203–209.
[28] S.J. Clough, A.F. Bent, Floral dip: a simplified method for *Agrobacterium*-mediated transformation of *Arabidopsis Thaliana*, Plant J. 16 (6) (1998) 735–743.
[29] T. Murashige, F. Skoog, A revised medium for rapid growth and bioassay with tobacco tissue cultures, Physiol. Plant. 15 (3) (1962) 473–497.
[30] M.-A. Tossounian, K. Wahni, I. Van Molle, D. Vertommen, L.A. Rosado, J. Messens, Redox-regulated methionine oxidation of *Arabidopsis Thaliana* glutathione Transferase Phi9 induces H-site flexibility, Pro. Scie. 28 (1) (2018) 56–67.
[31] V. Velikova, I. Yordanov, A. Edreva, Oxidative stress and some antioxidant systems in acid rain-treated bean plants, Plant Sci. 151 (1) (2000) 59–66.
[32] H. Liu, C. Yu, H. Li, B. Ouyang, T. Wang, J. Zhang, X. Wang, Z. Ye, Overexpression of Shdhn, A Dehydrin gene from solanum habrochaites enhances tolerance to multiple abiotic stresses in tomato, Plant Sci. 231 (November 2015) (2015) 198–211.
[33] V.E. Fadouloglou, M. Kokkinidis, N.M. Glykos, Determination of protein Oligomerization state: two approaches based on Glutaraldehyde crosslinking, Anal. Biochem. 373 (2) (2008) 404–406.
[34] S. Jacques, B. Ghesquière, P.-J. De Bock, H. Demol, K. Wahni, P. Willems, J. Messens, F. Van Breusegem, K. Gevaert, Protein methionine Sulfoxide dynamics in *Arabidopsis Thaliana* under oxidative stress, Mol. Cell. Proteomics 14 (5) (2015) 1217–1229.
[35] S. Wang, S. Sun, Z. Li, R. Zhang, J. Xu, Accurate de novo prediction of protein contact map by ultra-deep learning model, PLoS Comput. Biol. 13 (1) (2017) 1–34.
[36] J.P. Munyampundu, Y.P. Xu, X.Z. Cai, Phi class of glutathione S-Transferase gene superfamily widely exists in nonplant taxonomic groups, Evol. Bioinforma. 12 (2015) 59–71.
[37] L. Wang, X. Jin, Q. Li, X. Wang, Z. Li, X. Wu, Comparative proteomics reveals that phosphorylation of B carbonic anhydrase 1 might be important for adaptation to drought stress in *Brassica Napus*, Sci. Rep. 6 (39024) (2016), https://doi.org/10.1038/srep39024.
[38] P.G. Sappl, A.J. Carroll, R. Clifton, R. Lister, J. Whelan, A.H. Millar, K.B. Singh, The *Arabidopsis* glutathione Transferase gene family displays complex stress regulation and co-silencing multiple genes results in altered metabolic sensitivity to oxidative stress, Plant J. 58 (1) (2009) 53–68.
[39] D. Sheehan, G. Meade, V.M. Foley, C.A. Dowd, Structure, function and evolution of glutathione Transferases: implications for classification of non-mammalian members of an ancient enzyme superfamily, Biochem. J. 360 (Pt 1) (2001) 1–16.
[40] S. Contreras-Martos, H.H. Nguyen, P.N. Nguyen, N. Hristozova, M. Macossay-Castillo, D. Kovacs, A. Bekesi, J.S. Oemig, D. Maes, K. Pauwels, P. Tompa, P. Lebrun, Quantification of intrinsically disordered proteins: a problem not fully appreciated, Front. Mol. Biosci. 5 (2018) 83.
[41] J.M. Rainard, G.C. Pandarakalam, S.P. Mcelroy, Using microscale Thermophoresis to characterize hits from high-throughput screening: a European Lead factory perspective, Slas Discov. 23 (3) (2018) 225–241.
[42] J.R. Perkins, I. Diboun, B.H. Dessailly, J.G. Lees, C. Orengo, Transient protein-protein interactions: structural, functional, and network properties, Structure 18 (10) (2010) 1233–1243.
[43] R. Schweiger, J. Soll, K. Jung, R. Heermann, S. Schwenkert, Quantification of interaction strengths between chaperones and Tetratricopeptide repeat domain-containing membrane proteins, J. Biol. Chem. 288 (42) (2013) 30614–30625.
[44] P. Ahmad, M. Sarwat, S. Sharma, Reactive oxygen species, antioxidants and Signaling in plants, J. Plant Biol. 51 (3) (2008) 167–173.
[45] A. Mhamdi, G. Queval, S. Chaouch, S. Vanderauwera, F. Van Breusegem, G. Noctor, Catalase function in plants: a focus on *Arabidopsis* mutants as stress-mimic models, J. Exp. Bot. 61 (15) (2010) 4197–4220.
[46] I. Sharma, P. Ahmad, P. Ahmad (Ed.), Catalase: A Versatile Antioxidant in Plants, Elsevier Inc, 2014, pp. 131–148.
[47] M. Hara, M. Fujinaga, T. Kuboi, Radical scavenging activity and oxidative modification of Citrus Dehydrin, Plant Physiol. Biochem. 42 (7–8) (2004) 657–662.
[48] R. Mittler, S. Vanderauwera, N. Suzuki, G. Miller, V.B. Tognetti, K. Vandepoele, M. Gollery, V. Shulaev, F. Van Breusegem, Ros signaling: the new wave? Trends Plant Sci. 16 (6) (2011) 300–309.
[49] M. Ashraf, R. Rasheed, I. Hussain, M. Iqbal, M. Haider, S. Parveen, M. Asim, Hydrogen peroxide modulates antioxidant system and nutrient relation in maize (*Zea Mays* L.) under water deficit conditions, Arch. Agron. Soil Sci. 61 (4) (2015) 507–523.
[50] A. Hameed, N. Iqbal, Chemo-Priming With Mannose, Mannitol And H_2o_2 Mitigate Drought Stress In Wheat, 42 (2014), pp. 450–462.
[51] U. Wagner, R. Edwards, D.P. Dixon, F. Mauch, Probing the diversity of the *Arabidopsis* glutathione S-Transferase gene family, Plant Mol. Biol. 49 (5) (2002) 515–532.
[52] C. Frova, Glutathione Transferases in the genomics era: new insights and perspectives, Biomol. Eng. 23 (4) (2006) 149–169.
[53] K.A. Marrs, The functions and regulation of glutathione S-Transferase in plants, Annu. Rev. Plant Physiol. Plant Mol. Biol. 47 (1996) 127–158.
[54] E. Horváth, K. Bela, C. Papdi, Á. Gallé, L. Szabados, I. Tari, J. Csiszár, The role of *Arabidopsis* glutathione Transferase F9 gene under oxidative stress in seedlings, Acta Biol. Hung. 66 (4) (2015) 406–418.
[55] Y.E. Kim, M.S. Hipp, A. Bracher, M. Hayer-Hartl, F.U. Hartl, Molecular chaperone functions in protein folding and proteostasis, Annu. Rev. Biochem. 82 (2013) 323–355.
[56] S. Chakrabortee, C. Boschetti, L.J. Walton, S. Sarkar, D.C. Rubinsztein, A. Tunnacliffe, Hydrophilic protein associated with desiccation tolerance exhibits broad protein stabilization function, Proc. Natl. Acad. Sci. U. S. A. 104 (46) (2007) 18073–18078.
[57] P. Chien, L.M. Gierasch, Challenges and dreams: physics of weak interactions essential to life, Mol. Biol. Cell 25 (22) (2014) 3474–3477.
[58] L. Makowski, D.J. Rodi, S. Mandava, D.D.L. Minh, D.B. Gore, R.F. Fischetti, Molecular crowding inhibits intramolecular breathing motions in proteins, J. Mol. Biol. 375 (2) (2008) 529–546.
[59] S. Alberti, Cell adaptation upon stress: the emerging role of membrane-less compartments, Curr. Opin. Cell Biol. 47 (2017) 34–42.
[60] E.H. Mcconkey, Molecular evolution, intracellular organization, and the quinary structure of proteins, Pnas 79 (10) (1982) 3236–3240.
[61] R.D. Cohen, G.J. Pielak, A cell is more than the sum of its (dilute) parts: a brief history of quinary structure, Protein Sci. 26 (3) (2017) 403–413.
[62] S.J. Gilmour, N.N. Artus, M.F. Thomashow, Cdna sequence analysis and expression of two cold-regulated genes of *Arabidopsis Thaliana*, Plant Mol. Biol. 18 (1) (1992) 13–21.
[63] J. Klodmann, M. Senkler, C. Rode, H.P. Braun, Defining the protein complex proteome of plant mitochondria, Plant Physiol. 157 (2) (2011) 587–598.
[64] L.A. Del Río, E. López-Huertas, Ros generation in peroxisomes and its role in cell

Signaling, Plant Cell Physiol. 57 (7) (2016) 1364–1376.
[65] J. Ito, T.S. Batth, C.J. Petzold, A.M. Redding-Johanson, A. Mukhopadhyay, R. Verboom, E.H. Meyer, A.H. Millar, J.L. Heazlewood, Analysis of the Arabidopsis cytosolic proteome highlights subcellular partitioning of central plant metabolism, J. Proteome Res. 10 (4) (2011) 1571–1582.
[66] Z. Mcbride, D. Chen, C. Reick, J. Xie, D.B. Szymanski, Global analysis of membrane-associated protein Oligomerization using protein correlation profiling, Mol. Cell. Proteomics 16 (11) (2017) 1972–1989.
[67] B. Förster, C.B. Osmond, B.J. Pogson, Improved survival of very high light and oxidative stress is conferred by spontaneous gain-of-function mutations in Chlamydomonas, Biochim. Biophys. Acta 1709 (1) (2005) 45–57.
[68] S. Huang, O. Van Aken, M. Schwarzländer, K. Belt, A.H. Millar, The roles of mitochondrial reactive oxygen species in cellular signaling and stress response in plants, Plant Physiol. 171 (3) (2016) 1551–1559.
[69] A.J. Borysik, D. Kovacs, M. Guharoy, P. Tompa, Ensemble methods enable a new definition for the solution to gas-phase transfer of intrinsically disordered proteins, Jacs 137 (43) (2015) 13807–13817.